NUMERICAL SIMULATION OF UNSTEADY LOW-REYNOLDS-NUMBER SEPARATED FLOWS OVER AIRFOILS

Mahidhar Tatineni*and Xiaolin Zhong†
University of California, Los Angeles, California 90095

Abstract

Low-Reynolds-number flows over airfoils are characterized by the presence of separation bubbles. The separation bubbles are often unsteady and have a significant impact on the overall flowfield. This paper numerically simulates unsteady two dimensional low-Reynolds-number flows over airfoils and analyzes the instabilities associated with the separated flowfield. Unsteady laminar calculations of low-Reynolds-number flows over airfoils are performed using a Navier-Stokes solver. Laminar-turbulent calculations are also done for comparison. The studies show that separated flow is unstable and results in periodic vortex shedding. The time-averaged lift and drag coefficients are compared with the experimental values, and are in good agreement with the experimental results. Comparison with the results of a linear stability analysis, of the separated boundary layer, shows that the wavenumber and frequency in the numerical simulations agrees with the most unstable wavenumber and frequency from the linear stability analysis. Hence, the vortex shedding is linked to the Tollmien Schlichting instability wave of the separated boundary layer. An analysis of the numerical solutions also shows the interaction and growth of subharmonic waves, a possible path to transition.

INTRODUCTION

Low-Reynolds-number (in the range of $\mathrm{Re} = 5 \times 10^4$ to 1×10^6) aerodynamics is important for a variety of aircrafts, ranging from sailplanes and human-powered aircrafts to high altitude unmanned aerial vehicles(UAV's) [1,2]. There has been considerable research, both experimental [3–8] and computational [9–13], on low-Reynolds-number flows over airfoils. The current research is motivated by the planned flight tests, at NASA Dryden Flight Research Center, which will use the APEX high altitude aircraft to collect aerodynamic data in the transonic low-Reynolds-number flow regime [2].

In low-Reynolds-number flows, the flowfield is strongly influenced by the the presence of laminar-turbulent separation bubbles. Figure 1 shows a schematic of the structure of a separation bubble. The flow is laminar when the separation occurs due to the adverse pressure gradient. The separated boundary layer is unstable and rapidly undergoes transition. The turbulent flow reattaches, and the region between the separation point and the reattachment point is called the separation bubble. These bubbles are often unsteady and have significant effects on the overall flowfield.

Extensive experimental studies have been conducted [3–5,8], to evaluate the performance of airfoils in subsonic low-Reynolds-number flows, and they have shown the strong influence of the separation bubbles on the overall flowfield. The experimental investigations have also revealed the presence of dominant instability waves which amplify in accordance with the linear stability theory. Leblanc, Blackwelder, and Liebeck [6] showed that the peak frequencies measured in the velocity spectra for the instability region match the most amplified wavenumber and frequency scaling calculated by linear stability theory. Dovgal, Kozlov, and Michalke [7] investigated the linear instability and the nonlinear wave interactions in the separated regions. Their results also show the linear evolution of disturbances in the separation bubble. They also discussed the interactions of the nonlinear disturbances and the path to transition. A schematic of the various stages of transition is shown in Fig. 2.

Low-Reynolds-number separation bubbles include flows in both the subsonic and transonic Mach number regimes. Drela and Giles [14] used a viscous-inviscid approach to calculate transonic low-Reynolds-number flows. The simulations used an Euler formulation coupled with an integral boundary layer formulation, with a transition prediction formulation of e^n type. Their calculations show the strong influence of separation bubbles on the performance of the airfoils. Lin and Pauley [13] used an unsteady, incompressible Navier-Stokes approach to compute low-Reynolds-number flows. Their results show the unsteady nature of the separation bubble and the associated periodic vortex shedding. The dominant frequency was shown to be in agreement with the most amplified frequency from the linear stability analysis of a mixing layer corresponding to the separated boundary layer.

The present study considers numerical simulation and

*Graduate Student, Member AIAA

†Assistant Professor, Mechanical and Aerospace Engineering Department, Member AIAA

analysis of low-Reynolds-number compressible flows over airfoils. A detailed linear stability analysis of the separated flow is performed to explain the unsteady nature of the flow. Numerical results show an unsteady vortex shedding process, which is shown through a linear stability analysis to correspond to the instability of the separated boundary layer. The results confirm the linear evolution of disturbances in the separated region. Computations over the Eppler 387 airfoil and the APEX airfoil are the two cases considered. The APEX airfoil was designed at NASA Dryden for the planned high altitude flight tests [2]. The airfoil has been designed, using a low-Reynolds-number design code [14] to operate in the transonic low-Reynolds-number regime. For the flow over the Eppler 387 airfoil the time-averaged results are compared with the experimental data [8] and existing numerical results [13]. The results from the computations for the APEX airfoil are also presented. The computations are performed using both the laminar Navier-Stokes equations and the Favre averaged Navier-Stokes equations. For the laminar-turbulent calculations, the transition location is fixed and the Baldwin-Lomax algebraic eddy-viscosity model is used for turbulence modeling. A second order implicit Gauss-Seidel method is used for the calculations.

MATHEMATICAL FORMULATION

Governing Equations

The mass, momentum and energy conservation equations for compressible flows in two dimensions are as follows:

$$\frac{\partial U}{\partial t} + \frac{\partial F}{\partial x} + \frac{\partial G}{\partial y} = 0 \tag{1}$$

where

$$\mathbf{U} = \begin{bmatrix} \rho \\ \rho u \\ \rho v \\ e \end{bmatrix}, \tag{2}$$

$$\mathbf{F} = \begin{bmatrix} \rho u \\ \rho u^2 + p + \sigma_{11} \\ \rho uv + \sigma_{12} \\ u(e + p + \sigma_{11}) + \sigma_{12} v + q_1 \end{bmatrix}, \tag{3}$$

$$\mathbf{G} = \begin{bmatrix} \rho v \\ \rho uv + \sigma_{21} \\ \rho v^2 + p + \sigma_{22} \\ v(e + p + \sigma_{22}) + \sigma_{21} u + q_2 \end{bmatrix} \tag{4}$$

where σ_{ij} represents the shear stresses and q_1, q_2 are the heat conduction fluxes. The equation of state is as follows:

$$p = (\gamma - 1)\left[e - \frac{1}{2}\rho\left(u^2 + v^2\right)\right] \tag{5}$$

The viscosity coefficient is calculated using the Sutherland's law. The Prandtl number(Pr) is taken to be 0.7, and the ratio specific heats (γ) is taken as 1.4. No slip boundary conditions are imposed on the wall.

Turbulence Modeling

The majority of the results presented in this paper are from laminar computations. In addition laminar-turbulent calculations are also performed for comparison. For simplicity the two layer algebraic eddy viscosity model developed by Baldwin and Lomax [15] has been used for the turbulence modeling. The turbulent boundary layer is considered to be formed by two regions, with different expressions for the eddy viscosity coefficient. The eddy viscosity in the inner region is given by the Prandtl-Van Driest formulation

$$\mu_i = \rho(KYD)^2|\omega| \tag{6}$$

where ρ is the density, $|\omega|$ is the magnitude of the vorticity, K=0.40 is the von Karman's constant and Y represents the normal distance from the wall. D is the Van Driest damping factor. The eddy viscosity in the outer region is given by

$$\mu_o = \rho k C_{cp} Y_{max} F_{max} F_{kleb} \tag{7}$$

where

$$F_{max} = max(Y|\omega|D) \tag{8}$$

and F_{kleb} is the klebanoff intermittency correction given by

$$F_{kleb} = [1 + 5.5(C_{kleb} Y / Y_{max})]^{-1} \tag{9}$$

where C_{kleb} is a constant. Details of the model can be found in Baldwin and Lomax [15]. In the laminar-turbulent calculations the turbulence model is used after the transition location.

Transition Prediction

For low-Reynolds-number flows over airfoils, the separated laminar boundary layer may undergo transition. Hence, a transition prediction method is required. For the current laminar-turbulent calculations the transition is fixed. However, for future calculations an approximate e^n will be used for transition prediction.

NUMERICAL METHOD

In the computations the equations are transformed from the Cartesian coordinates(x,y,t) into the curvilinear computational coordinates(ξ,η,τ). The computations are performed on a C-grid (for airfoil computations).The grids are generated using an elliptic grid generator. An implicit second order finite volume line Gauss-Seidel iteration method [16] is used for the computations. The inviscid terms are computed using the flux splitting method and central differencing is used for the viscous terms. The computation involves calculations which are implicit in the η (normal) direction, while the ξ (streamwise) direction terms are computed by a line Gauss-Seidel iteration with alternating

sweeps in the backward and forward ξ directions. The computations are first order accurate in time, with the time step being small enough to resolve the time dependence of the solution. This is checked by using smaller timesteps and confirming that the solution is independent of the timestep used. The calculations were performed with grids of 158×58 and 314×114 to ensure the grid independence of the solution. The averaged lift and drag coefficients from the two solutions are within 3% of each other.

RESULTS

The time accurate Navier-Stokes solver is used to calculate unsteady separated low-Reynolds-number flows over the Eppler 387 airfoil and the APEX airfoil. The results for the Eppler 387 airfoil are compared with existing experimental and computational results. A linear stability analysis is performed for the separated boundary layer in both the cases. The results are compared with the numerical observations.

Validation Cases

The laminar Navier-Stokes solver is validated by computing the incompressible flat plate boundary layer flow. The results are in good agreement with the Blasius boundary layer solution. The turbulence model was validated by computing fully turbulent flow over the NACA 0012 airfoil for the following flow conditions: Re $= 9 \times 10^6$, $\alpha = 1.49^o$, $M = 0.7$. The results are compared with existing numerical results [17]. The c_l value is calculated to be 0.23, which is within 4% of the reference value of 0.2401. The c_d value is calculated to be 0.0082, which is within 2.5% of the reference value of 0.0084.

The Eppler 387 Airfoil

Low-Reynolds-number flow over the Eppler 387 airfoil is calculated for the following flow conditions: Re $= 1 \times 10^5$, $\alpha = 1^o$, M $= 0.2$ The 314×114 grid used for the computations is shown in Fig. 3. Both laminar and turbulent calculations are considered for this case. The calculations show the unsteady nature of the flow, caused due to the instability of the separated boundary layer.

The time-averaged results are compared with existing experimental data [8]. Table 1 shows the comparison of the time-averaged lift coefficient with the experimental value. The time averaged lift-coefficient is found to compare well with experimental results for both the laminar and turbulent solutions. The time-averaged drag coefficient is compared with the experimental data in Table 2. The drag coefficient from the turbulent calculation agrees well with the experimental result. The larger drag in the laminar case is found to be due to a larger separation bubble predicted in the laminar calculations.

Table 1: **Comparison of averaged lift coefficients with experimental data.**

	c_l	% Error
Experimental	0.4910	–
Laminar	0.4515	8.05
Turbulent	0.4712	4.04

Table 2: **Comparison of averaged drag coefficients with experimental data.**

	c_d	% Error
Experimental	0.0183	–
Laminar	0.0218	19.12
Turbulent	0.0189	3.28

The time-averaged surface pressure distribution agrees well with the experimental results for both the calculations, as shown in Fig. 4. Hence, the time-averaged results from both approaches are similar and agree well with the experimental values.

The numerical solution shows that the flow is unsteady, with periodic vortex shedding. The vortex shedding process is visualized in Fig. 5 using six instantaneous flowfield streamline plots in sequence, corresponding to one time period. The plots also show the existence of a dominant wavenumber in the numerical results. This unsteadiness in the flowfield is in agreement with the results of Lin and Pauley [13], who extensively studied incompressible flows over the Eppler 387 airfoil and found similar unsteady vortex shedding. The unsteady nature of the flow is evident from the time variation of the surface pressure, at a point located near the trailing edge, as shown in Fig. 6. The unsteady nature of the flowfield causes a corresponding unsteady variations in the lift and drag coefficients. The variation of the instantaneous lift and drag coefficients with time is is shown in Fig. 7 and Fig. 8 respectively. Both the figures show the unsteady nature of the flow. In addition, the presence of a dominant frequency in the flow is also seen.

The time-averaged flowfield shows the presence of the separation bubble. The large scale characteristics of the time-averaged separation bubble are similar for the laminar and turbulent solutions, as seen from Fig. 9 and Fig. 10. Figure 11 shows the average velocity profile at several locations on the upper surface of the airfoil. The reverse flow region within the separation bubble can be clearly seen.

The source of the unsteady nature of the flowfield is ascertained using a linear stability analysis of the separated flowfield using the time-averaged solution as the

mean velocity profile, as shown in Fig. 11 The analysis shows that the boundary layer is unstable for a range of wave numbers. The growth rates and frequencies corresponding to the various wavenumbers are given in Table 3 and plotted in Fig. 12 and Fig. 13. The maximum

Table 3: **Results of the linear stability analysis of the separated flow for the Eppler 387 airfoil case.**

Wavenumber $\alpha^* = \alpha\delta^*$	Frequency $\omega_R^* = \frac{\omega_R\delta^*}{U_\infty}$	Growth Rate $\omega_I^* = \frac{\omega_I\delta^*}{U_\infty}$
.01107	.00457	.00209
.03320	.01383	.00713
.04427	.01849	.00940
.06322	.02647	.01260
.06640	.02781	.01304
.07747	.03244	.01431
.08854	.03705	.01516
.09961	.04160	.01556
.11067	.04609	.01549
.12174	.05051	.01492
.13281	.05484	.01382
.14387	.05907	.01219
.16601	.06718	.00721

growth rate occurs at $\alpha^* = 0.1$, where α^* is the nondimensional wavenumber. The wavenumber is nondimensionalized as $\alpha^* = \alpha\delta^*$, where $\delta^* = x/(\sqrt{Re_x})$, $Re_x = \frac{\rho_\infty U_\infty x}{\mu_\infty}$. The numerical results are expected to correspond to the most unstable wavenumber. Figure 14 shows the instantaneous pressure coefficient distribution obtained from the numerical solution. The wavenumber corresponding to the numerical simulations can be determined from this data. The nondimensional wavenumber is found to be 0.098, which is within 2% of the value value calculated from linear stability theory. The result is also consistent with the experimental observations by Leblanc et al. [6] that the dominant frequencies measured in the velocity spectra correspond to the most unstable wavenumber from the linear stability analysis of the inflectional velocity profiles. Figure 15 shows the frequency spectrum of the unsteady solution at various locations on the surface of the airfoil. For the locations in the separation bubble, the dominant frequency is $\omega^* = 0.039$. This is within 6.5% of the frequency predicted by linear stability theory. This is consistent with the results of Lin and Pauley [13] who compared the dominant frequency in the numerical simulations with the most amplified frequency from a stability analysis, of a mixing layer representative of the separated boundary layer. Figure 15 also shows the interaction of 2-D fundamental and subharmonic waves. The results show that a subharmonic disturbances are generated by the fundamental wave. This is expected to lead to nonlinear and three dimensional effects and subsequently, transition. The result is also consistent with experimental observations of interactions within the separation bubble by Dovgal et al [7]. In this region three dimensional effects are expected to be important, and a localized three dimensional calculation will be required to resolve the flowfield [18].

The APEX Airfoil

The flow over the APEX airfoil was calculated for the following freestream conditions: $\alpha = 4^o, M = 0.5, Re = 2 \times 10^5$. The 300×58 grid used for the computations is shown in Fig. 16. The numerical simulations reveal an unsteady vortex shedding process similar to the Eppler 387 case. Figure 17 shows the time-averaged structure of the separation bubble. The region of reverse flow in the separation bubble can be clearly seen. Hence, the mean velocity profiles will have an inflection point, and are expected to be inviscidly unstable. Figure 18 shows the inflectional velocity profile used for the linear stability calculations. The analysis shows that the separated boundary layer is unstable for a range of wavenumbers. The growth rates and frequencies are tabulated below and also plotted in Figures 19 and 20. The most unstable nondimensional wavenumber from linear stability theory is found to be 0.16. The numerical value for the same is 0.147, which is within 8.5% of the ex-

Table 4: **Results of the linear stability analysis of the separated flow for the APEX airfoil case**

Wavenumber $\alpha^* = \alpha\delta^*$	Frequency $\omega_R^* = \frac{\omega_R\delta^*}{U_\infty}$	Growth Rate $\omega_I^* = \frac{\omega_I\delta^*}{U_\infty}$
.02370	.00036	.00185
.03160	.00269	.00398
.04740	.00871	.00876
.06320	.01580	.01339
.07900	.02354	.01744
.09480	.03167	.02080
.11060	.04000	.02344
.12640	.04836	.02535
.14220	.05665	.02656
.15800	.06480	.02709
.17380	.07273	.02697
.18960	.08040	.02622
.20540	.08778	.02487
.22120	.09485	.02293
.23700	.10158	.02043
.25280	.10795	.01737
.26860	.11394	.01377
.28440	.11954	.00966
.30020	.12473	.00504
.30810	.12717	.00255

pected value. Further computations and analysis are in progress to study flows over the APEX airfoils.

CONCLUDING REMARKS

Unsteady low-Reynolds-number flows over the Eppler 387 and APEX airfoils have been numerically simulated. Both the studies show the unsteady nature of the separated flow, with periodic vortex shedding. The vortex shedding seen in numerical results is found to be due to the inviscid instability of the separated boundary layer. The characteristics of the laminar region of the separation bubble are found to be in good agreement with the linear stability results. The numerical solutions also show that beyond a certain location in the separation bubble there is interaction between the fundamental and subharmonic waves. Hence, three dimensional and nonlinear effects may become important. Further computations are required to ascertain these effects. Future work will be directed towards localized three dimensional calculations to study the nonlinear effects.

ACKNOWLEDGMENTS

This research has been supported by NASA Dryden Flight Research Center under Grant NCC 2-374.

References

[1] Lissman , P. "Low Reynolds number airfoils". *Annual Review of Fluid Mechanics*, 1983, pp. 223–239.

[2] Murray , J., Moes , T., K.Norlin , J.Bauer , Geenen , R., Moulton , B., and Hoang. , S. "Piloted simulation study of a balloon-assisted deployment of an aircraft at high altitude.". *NASA-TM 104245*, 1992.

[3] Mueller , T. *Low Reynolds number vehicles.* AGARD-AG 288, 1985.

[4] Arena , A. and Mueller , T. "Laminar Separation, transition, and turbulent reattachment near the leading edge of airfoils". *AIAA Journal*, Vol. 18(7), 1980, pp. 747–753.

[5] Mueller , T. and Batill , S. "Experimental studies of separation on two-dimensional airfoil at low Reynolds numbers". *AIAA Journal*, Vol. 20(4), 1982, pp. 457–463.

[6] Leblanc , P., Blackwelder , R., and Liebeck. , R. *A comparison between boundary layer measurements in a laminar separation bubble flow and linear stability theory calculations.* Low Reynolds number aerodynamics: Proceedings of the Conference,Notre Dame, IN., June 5-7, 1989.Springer-Verlag, 1989.

[7] Dovgal , A. V., Kozlov , V. V., and Michalke , A. "Laminar Boundary Layer Separation:Instability and Associated Phenomena". *Progress of Aerospace Sciences*, Vol. 30, 1994, pp. 61–94.

[8] McGhee , R., Walker , B., and Millard , B. "Experimental Results for the Eppler 387 Airfoil at Low Reynolds Numbers in the Langley Low-Turbulence Pressure Tunnel". *NASA TM4062*, 1988.

[9] Choi , D. and Kang , D. "Calculation of Separation Bubbles Using a Partially Parabolized Navier-Stokes Procedure". *AIAA Journal*, Vol. 29(8), 1991, pp. 1266–1272.

[10] Drela , M. and Giles. , M. "Viscous-Inviscid analysis of transonic and low Reynolds number airfoils". *AIAA Journal*, Vol. 25(10), 1987, pp. 1347–1355.

[11] Schneider , J. and Ewald. , B. *Integration of linear stability methods into Navier-Stokes solvers for computation of transonic laminar airfoils.* AIAA Paper 94-1849-CP, 1994.

[12] Vatsa , V. and Carter , J. "Analysis of Airfoil Leading-Edge Separation Bubbles". *AIAA Journal*, Vol. 22(12), 1984, pp. 1697–1704.

[13] Lin , J. M. and Pauley , L. L. "Low-Reynolds-Number Separation on an Airfoil". *AIAA Journal*, Vol. 34(8), 1996, pp. 1570–1577.

[14] Drela , M. "Transonic Low-Reynolds Number Airfoils". *Journal of Aircraft*, Vol. 29(6), 1992, pp. 1106–1113.

[15] Baldwin , B. and Lomax. , H. *Thin Layer Approximation and Algebraic Model for Separated Turbulent Flows.* AIAA Paper 78-257, 1978.

[16] MacCormack , R. *Current Status of Numerical Solution of the Navier Stokes Equations.* AIAA Paper 85-0032, 1985.

[17] King , L. S. *A comparison of Turbulence Closure Models for Transonic Flows About Airfoils.* AIAA Paper 87-0418, 1987.

[18] Yang , Z. and Voke , P. R. *Numerical Study of Mechanisms of Boundary Layer Transition After a Separation Bubble.* Advances in Turbulence VI, 55-58, Kluwer Academic Publishers, 1996.

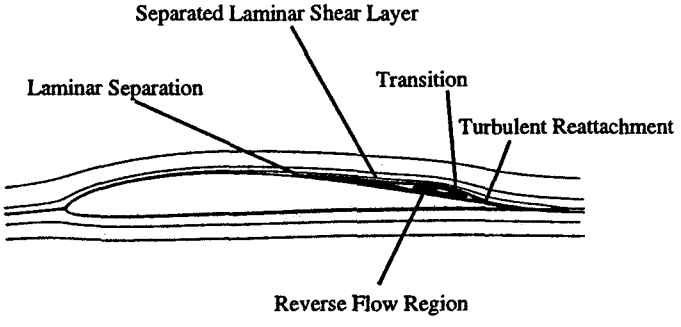

Figure 1: **Structure of the separation bubble for low Reynolds number flows.**

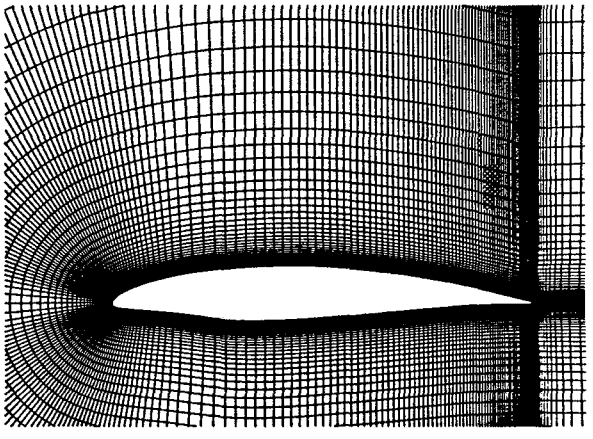

Figure 3: **A section of the 314 x 114 grid used for the computations over the Eppler 387 airfoil.**

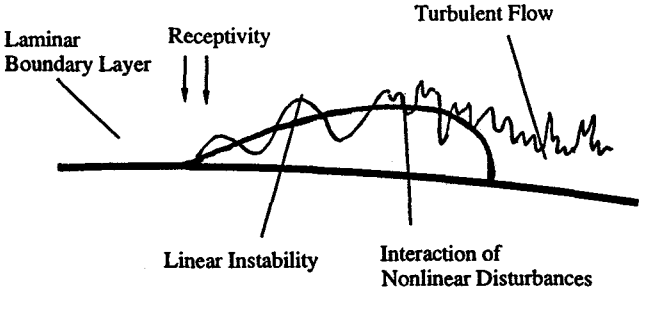

Figure 2: **A schematic showing the various stages of the transition process.**

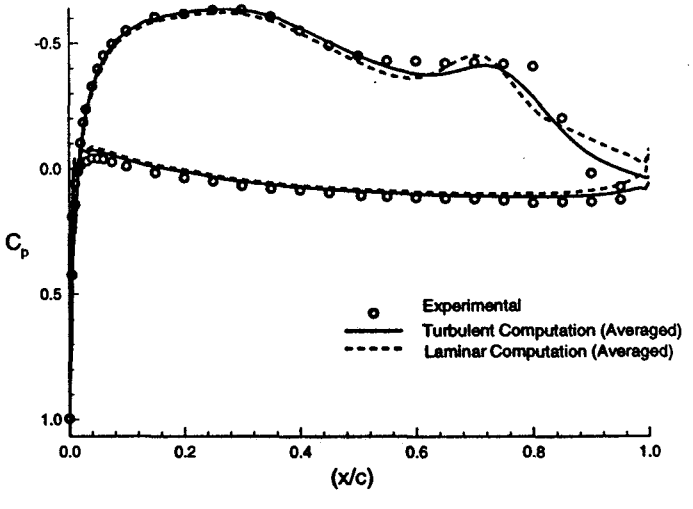

Figure 4: **Time averaged C_p distributions for the laminar and turbulent solutions compared with experimental results. Flow over the Eppler 387 airfoil at M=0.2, Re $= 1 \times 10^5$, $\alpha = 1°$.**

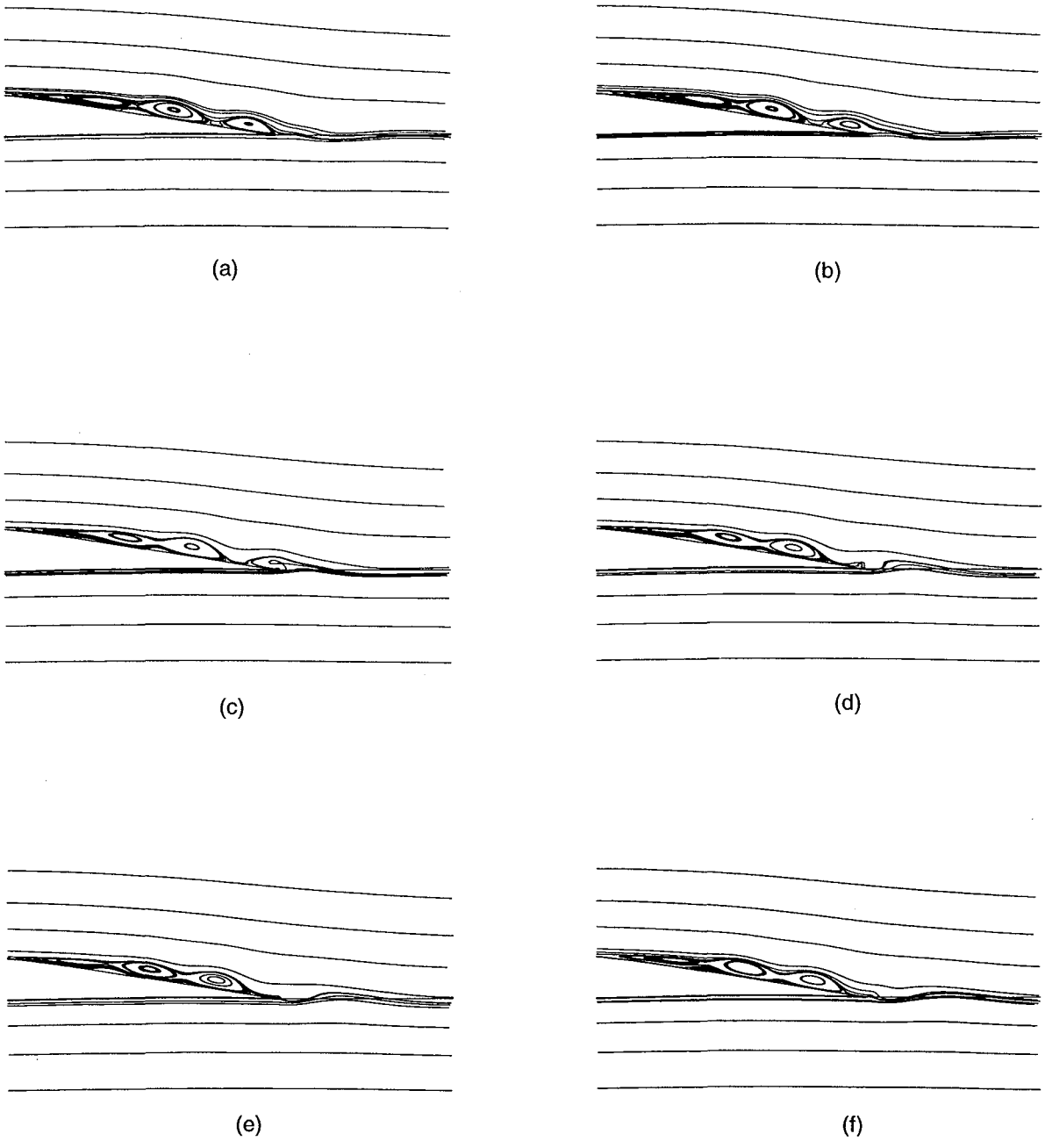

Figure 5: **Flowfield streamline plots (a)-(f) in sequence, corresponding to one time period, showing the vortex shedding process. Flow over the Eppler 387 airfoil at M=0.2, Re $= 1 \times 10^5$, $\alpha = 1°$.**

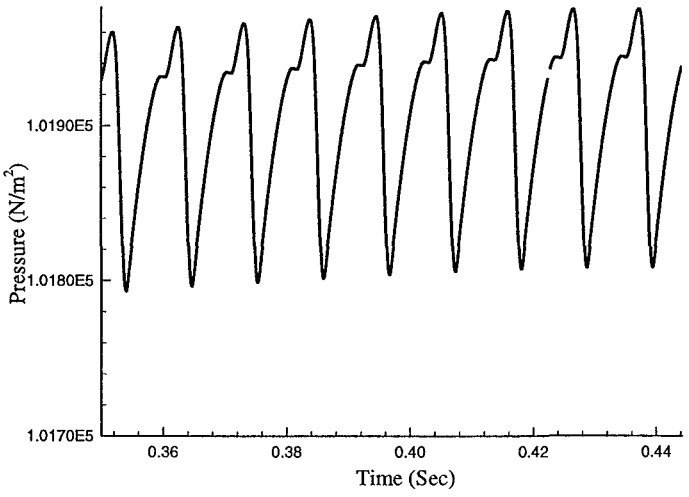

Figure 6: **The variation of surface pressure at a fixed point, near the trailing edge, with time. Flow over the Eppler 387 airfoil at M=0.2, Re=1×10^5, $\alpha = 1°$.**

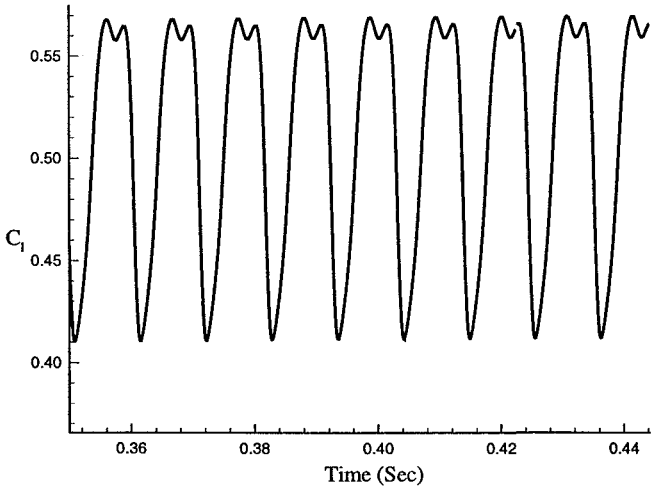

Figure 7: **The variation of the lift coefficient with respect to time. Flow over the Eppler 387 airfoil at M=0.2, Re $= 1 \times 10^5$, $\alpha = 1°$.**

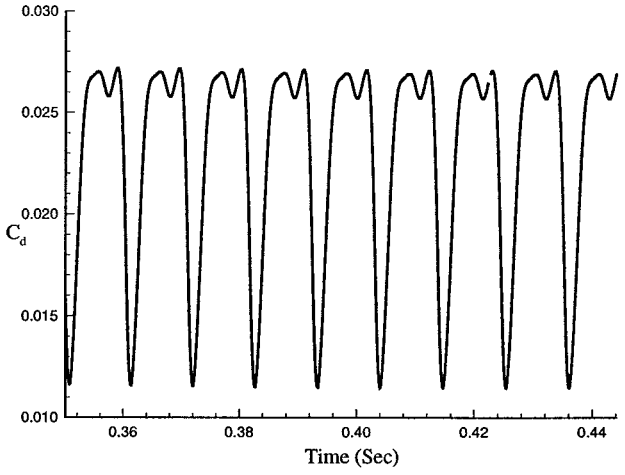

Figure 8: **The variation of the drag coefficient with respect to time. Flow over the Eppler 387 airfoil at M=0.2, Re $= 1 \times 10^5$. $\alpha = 1°$.**

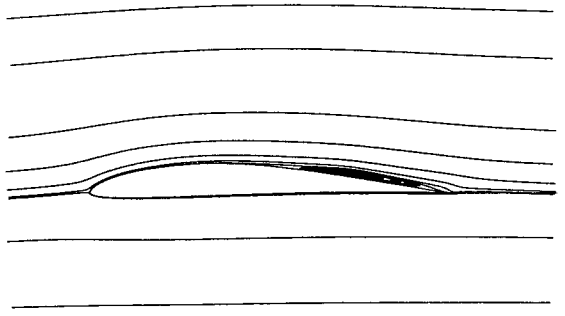

Figure 9: **Time-averaged streamlines for the laminar solution showing the separation bubble. Flow over the Eppler 387 airfoil at M=0.2. Re $= 1 \times 10^5$. $\alpha = 1°$.**

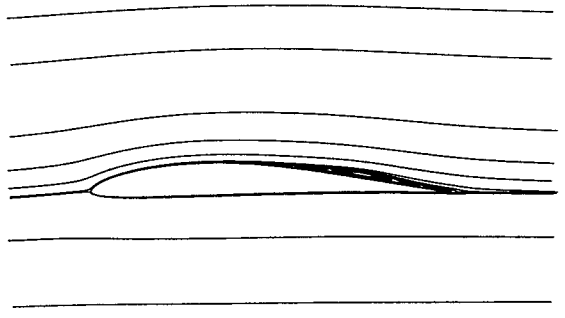

Figure 10: **Time-averaged streamlines for the turbulent solution showing the separation bubble. Flow over the Eppler 387 airfoil at M=0.2, Re $= 1 \times 10^5$, $\alpha = 1°$.**

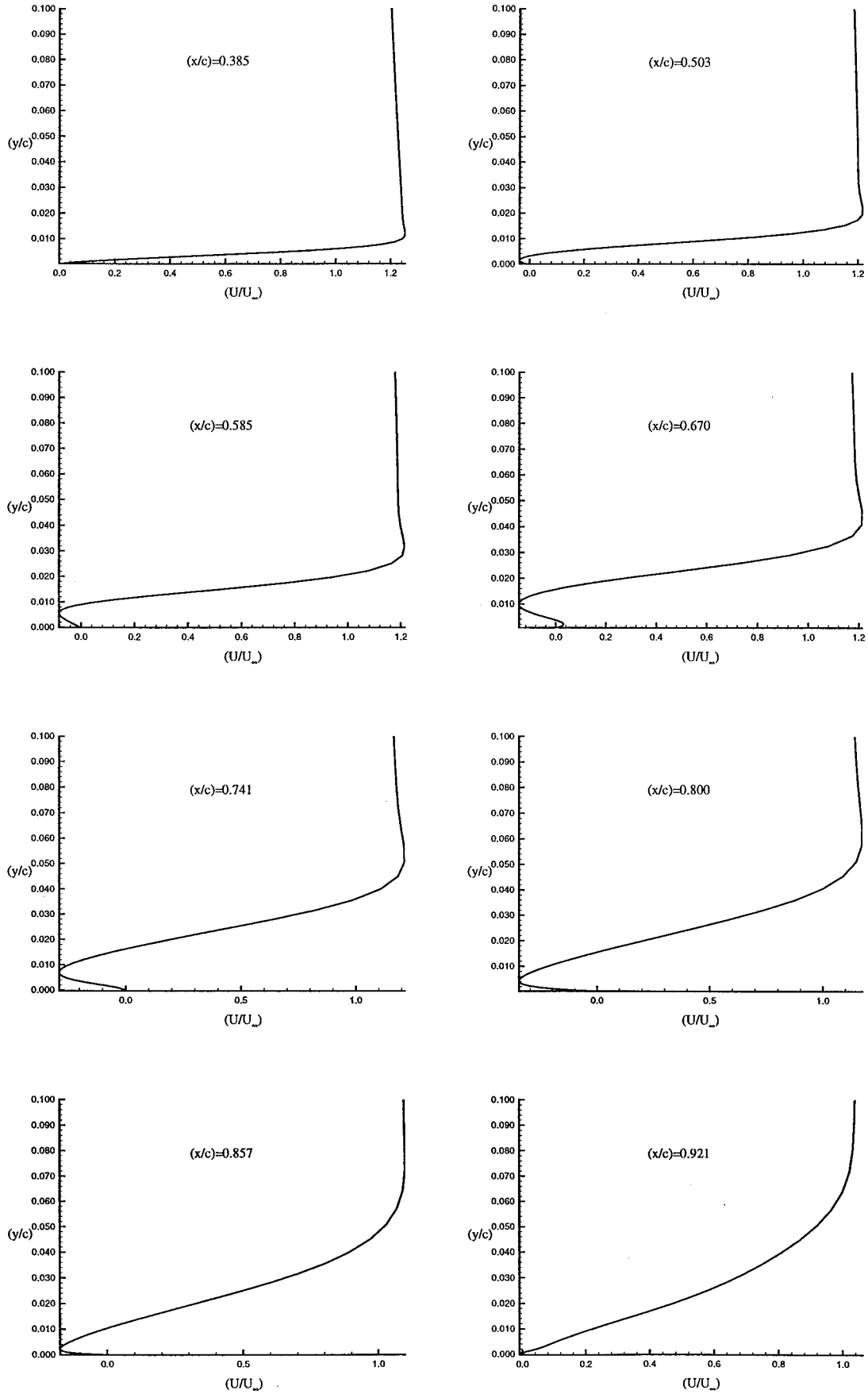

Figure 11: **Time-averaged velocity profiles at various locations on the upper surface of the airfoil. Flow over the Eppler 387 airfoil at M=0.2, Re = 1×10^5, $\alpha = 1^o$.**

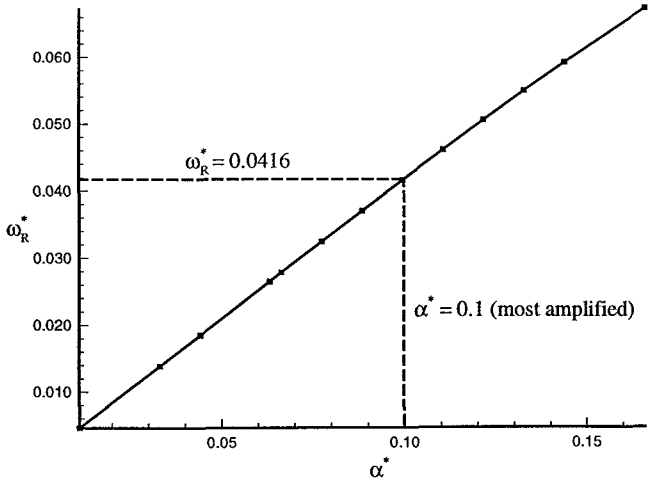

Figure 12: **The variation of the frequency with wavenumbers. Results obtained from the linear stability analysis. $\alpha^* = \alpha\delta^*$, $\omega_R^* = \omega_R \frac{\delta^*}{U_\infty}$. Flow over the Eppler 387 airfoil at M=0.2, Re $= 1 \times 10^5$, $\alpha = 1^o$.**

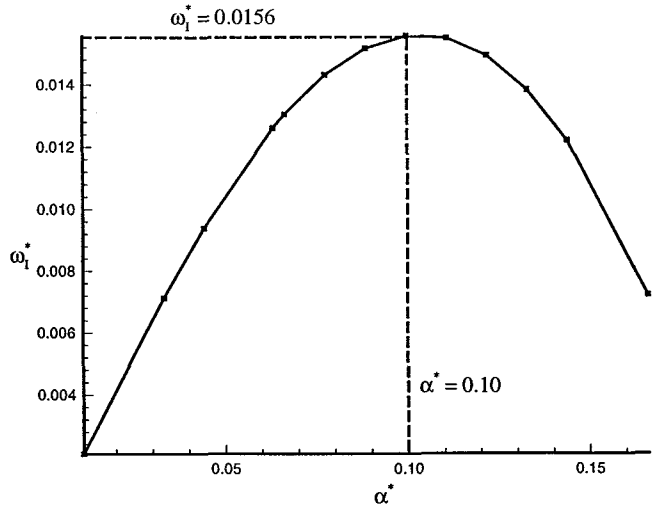

Figure 13: **The variation of the growth rates with wavenumbers. Results obtained from the linear stability analysis. $\alpha^* = \alpha\delta^*$, $\omega_I^* = \omega_I \frac{\delta^*}{U_\infty}$. Flow over the Eppler 387 airfoil at M=0.2, Re $= 1 \times 10^5$, $\alpha = 1^o$.**

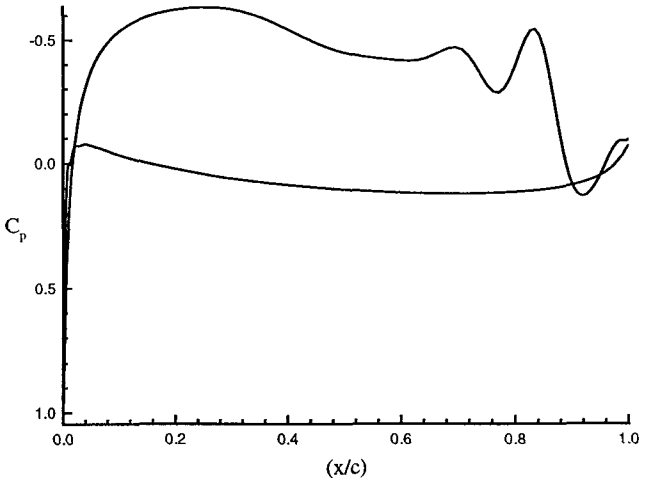

Figure 14: **Instantaneous pressure coefficient (C_p) distribution. Flow over the Eppler 387 airfoil at M=0.2, Re $= 1 \times 10^5$, $\alpha = 1^o$.**

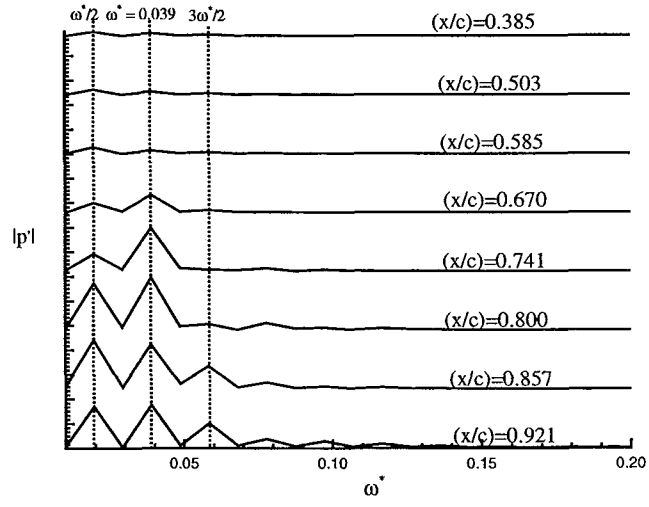

Figure 15: **Frequency spectrum of the pressure disturbance at various locations on the upper surface of the**

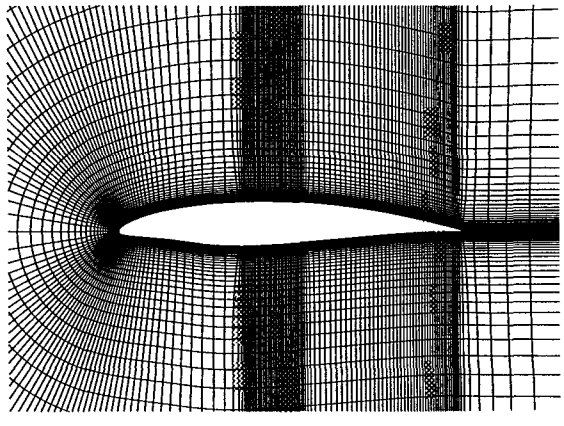

Figure 16: **The 300 x 58 grid used for computations of flow over the APEX airfoil.**

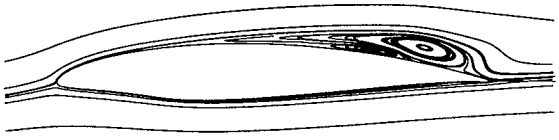

Figure 17: **Time-averaged streamlines showing the separation bubble. Flow over the APEX airfoil at M=0.5, Re $= 2 \times 10^5$, $\alpha = 4^o$.**

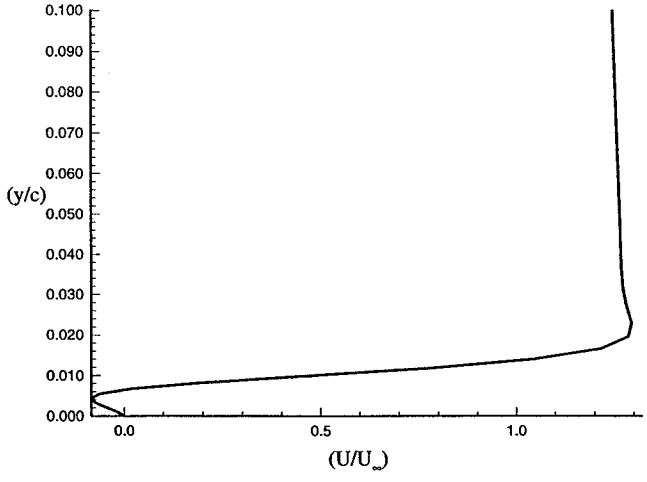

Figure 18: **The separated velocity profile used for linear stability calculations. Flow over the APEX airfoil at M=0.5, Re $= 2 \times 10^5$, $\alpha = 4^o$.**

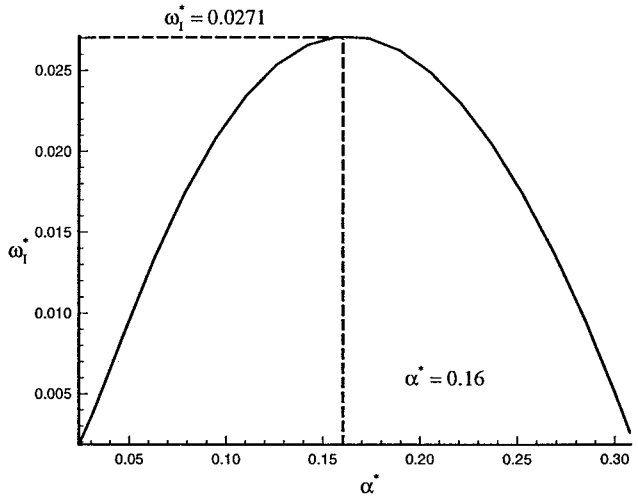

Figure 19: **The variation of the growth rates with wavenumbers. Results obtained from the linear stability analysis. $\alpha^* = \alpha\delta^*$, $\omega_I^* = \omega_I \frac{\delta^*}{U_\infty}$. Flow over the APEX airfoil at M=0.5, Re $= 2 \times 10^5$, $\alpha = 4^o$.**

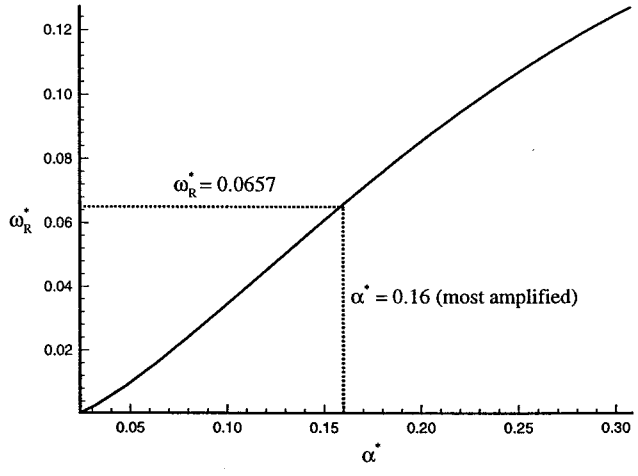

Figure 20: **The variation of the growth rates with wavenumbers. Results obtained from the linear stability analysis. $\alpha^* = \alpha\delta^*$, $\omega_I^* = \omega_I \frac{\delta^*}{U_\infty}$. Flow over the APEX airfoil at M=0.5, Re $= 2 \times 10^5$, $\alpha = 4^o$.**